The structure and activation of substrate water molecules in the S2 state of photosystem II studied by hyperfine sublevel correlation spectroscopy

ARTICLE *in* ENERGY & ENVIRONMENTAL SCIENCE · JUNE 2012

Impact Factor: 20.52 · DOI: 10.1039/C2EE21210B

6 AUTHORS, INCLUDING:

Sergey Milikisiyants
Rensselaer Polytechnic Institute
12 PUBLICATIONS **81** CITATIONS
SEE PROFILE

Ruchira Chatterjee
Lawrence Berkeley National Laboratory
24 PUBLICATIONS **159** CITATIONS
SEE PROFILE

Faisal Hammad Mekky Koua
University of Virginia
20 PUBLICATIONS **90** CITATIONS
SEE PROFILE

K. V. Lakshmi
Rensselaer Polytechnic Institute
78 PUBLICATIONS **2,408** CITATIONS
SEE PROFILE

Energy & Environmental Science

Cite this: *Energy Environ. Sci.*, 2012, **5**, 7747

www.rsc.org/ees

PAPER

The structure and activation of substrate water molecules in the S_2 state of photosystem II studied by hyperfine sublevel correlation spectroscopy†‡

Sergey Milikisiyants,[a] Ruchira Chatterjee,[a] Christopher S. Coates,[a] Faisal H. M. Koua,[b] Jian-Ren Shen[b] and K. V. Lakshmi*[a]

Received 25th January 2012, Accepted 19th April 2012
DOI: 10.1039/c2ee21210b

The water-splitting protein, photosystem II, catalyzes the light-driven oxidation of water to dioxygen. The solar water oxidation reaction takes place at the catalytic center, referred to as the oxygen-evolving complex, of photosystem II. During the catalytic cycle, the oxygen-evolving complex cycles through five distinct intermediate states, S_0–S_4. In this study, we trap the oxygen-evolving complex in the S_2 intermediate state by low temperature illumination of photosystem II isolated from three different species, *Thermosynechococcus vulcanus*, the PsbB variant of *Synechocystis* PCC 6803 and spinach. We apply two-dimensional hyperfine sublevel correlation spectroscopy to detect weak magnetic interactions between the paramagnetic tetra-nuclear manganese cluster of the S_2 state of the OEC and the surrounding protons. We identify five groups of protons that are interacting with the tetra-nuclear manganese cluster. From the values of hyperfine interactions and using the recently reported 1.9 Å resolution X-ray structure of the OEC in the S_1 state [Umena *et al.*, *Nature*, 2011, **473**, 55], we discuss the assignments of the five groups of protons and draw important conclusions on the structure of the oxygen-evolving complex in the S_2 state. In addition, we conclude that the structure of OEC is nearly identical in photosystem II from *Thermosynechococcus vulcanus*, the PsbB variant of *Synechocystis* PCC 6803 and spinach.

[a]*Department of Chemistry and Chemical Biology and The Baruch '60 Center for Biochemical Solar Energy Research, Rensselaer Polytechnic Institute, Troy, NY 12180, USA. E-mail: lakshk@rpi.edu; Fax: +1 (518) 276 4887; Tel: +1 (518) 276 3271*
[b]*Division of Bioscience, Graduate School of Natural Science and Technology and Faculty of Science, Okayama University, Okayama 700-8530, Japan*

† This study is supported by the Photosynthetic Systems Program, Office of Basic Energy Sciences, United States Department of Energy (DE-FG02-07ER15903).

‡ Electronic supplementary information (ESI) available. See DOI: 10.1039/c2ee21210b

Broader context

There is an urgent quest for environmentally benign, carbon neutral and sustainable energy. Nature converts solar energy to chemical energy using a process called photosynthesis which can provide elegant solutions to the inherent complexities of solar energy conversion and storage. In photosynthesis, two photoreactions take place prior to carbon fixation. In the first photoreaction the photosynthetic protein, photosystem II (PSII), catalyzes one of the most energetically demanding reactions by using light to oxidize water. The four-electron reaction involves the deprotonation of two substrate water molecules and the formation of dioxygen at the tetranuclear manganese-calcium–oxo (Mn_4Ca–oxo) of PSII. The activation of the substrate water molecules is exquisitely tuned by the catalytic Mn_4Ca–oxo cluster and the surrounding protein environment. It is important to elucidate the mechanism of water oxidation for the design of a new generation of bio-inspired catalytic systems. However, the mechanistic aspects of water oxidation have been elusive due to the inability of conventional methods to directly probe the reaction. During the catalytic reaction, PSII cycles through five distinct intermediates, S_0–S_4. In the present study, we use 2D ^{1}H HYSCORE spectroscopy to probe the structure and activation of the substrate water molecules that are directly coordinated to the Mn_4Ca–oxo cluster in the S_2 intermediate of PSII.

Introduction

There is an urgent quest for alternate, clean, environmentally benign, carbon neutral and sustainable sources to meet the rapidly growing global consumption of and demand for energy. With fossil fuels approaching peak production and more importantly, the ensuing effects of the use of these fuels on the environment, there is an ever increasing and imminent need to look to Nature for answers to the inherent complexities of energy conversion and storage. Nature converts solar energy to chemical energy using a process called photosynthesis. In photosynthesis, two photoreactions take place prior to carbon fixation in plants and cyanobacteria.[1–4] The first photoreaction takes place in the photosynthetic reaction center, photosystem II (PSII), where water is oxidized to dioxygen, protons and electrons. The second photoreaction occurs in the photosystem I (PSI) reaction center where the reducing equivalents required for the carbon fixation reactions are generated and stored as NADPH or 'biohydrogen'.

The solar water-splitting protein, PSII, catalyzes one of the most energetically demanding reactions known to mankind by using light energy to drive a catalyst capable of oxidizing water to dioxygen. The solar water oxidation reaction takes place at the catalytic center, referred to as the oxygen-evolving complex (OEC).[2,5–8] The four-electron water oxidation reaction involves the systematic deprotonation of two substrate water molecules and the formation of dioxygen and reducing equivalents at the tetranuclear manganese-calcium–oxo (Mn_4Ca–oxo) cluster in the OEC. The activation of the substrate water molecules is exquisitely tuned and controlled by the catalytic Mn_4Ca–oxo cluster in concert with a redox-active tyrosine residue (D1-Tyr161) and the smart matrix effects of the surrounding protein environment in the OEC. These effects are central to the water-oxidation chemistry of PSII. Elucidating the water-oxidation chemistry of PSII is of major importance in designing a new generation of bio-inspired catalytic systems for solar fuels production. However, the mechanistic aspects of the water oxidation reaction have been elusive due to the inability of conventional methods to directly probe the OEC. A major challenge is to develop methods to investigate the substrate water molecules at the Mn_4Ca–oxo cluster in the OEC of PSII.

During the catalytic reaction the Mn_4Ca–oxo cluster cycles through five distinct S-state (or charge-storage) photochemical intermediates, S_0–S_4, that results in the oxidation of the substrate water molecules.[9] It is imperative to understand the molecular and electronic structure of the OEC and, in particular, the fate of the substrate water molecules and the Mn_4Ca–oxo cluster in each of the S-state intermediates to elucidate the requirements for minimizing the energetic penalty for solar water oxidation. The OEC of PSII has been studied extensively by structural, spectroscopic, biochemical and computational methods.[8,10–24] While single crystal X-ray diffraction has provided important insight on the molecular geometry of the OEC in the stable S_1 state,[10–13,25] a high-resolution structure of the S_1 state was obtained recently after dramatic improvements in sample preparation and methodology.[24] Based on the latest X-ray crystal structure, the Mn_4Ca–oxo cluster consists of three manganese and a calcium ion that form a distorted cubane with μ-oxo bridges and a fourth manganese ion that is a dangler which is also linked to the cubane through μ-oxo bridges. The major breakthrough of this structure was the identification of all of the ligands including μ-oxo-atoms that are coordinated to the metal ions in the Mn_4Ca–oxo cluster. Most importantly, four water molecules were identified among the ligands: two water molecules are ligated to the dangler manganese ion and the other two water molecules are ligated to the Ca^{2+} ion in the S_1 state of the OEC.[24] The X-ray crystal structure has been further refined using advanced DFT calculations. However, only small changes have been observed in the refined structure.[26]

The structure of the S-state intermediates of the OEC has also been investigated by electron paramagnetic resonance (EPR), electron nuclear double resonance (ENDOR), electron spin echo envelope modulation (ESEEM), X-ray absorption and Fourier transform infrared (FTIR) spectroscopy.[18–20,23,27–33] Notably, X-ray spectroscopy has provided measurements of the metal-to-metal distances in the Mn_4Ca–oxo cluster. The geometry of the Mn_4Ca–oxo cluster was reported in the S_1 state and based on this data structural changes have been suggested upon advancement to higher intermediates, namely, the S_2 and S_3 states.[23,27,34] However, the metal-to-metal distances within the Mn_4Ca–oxo cluster deduced by X-ray spectroscopy are not compatible with the recent high-resolution X-ray crystal structure.[24]

In conjunction with X-ray diffraction, EPR and X-ray spectroscopy, recent density functional theory (DFT) and quantum mechanical/molecular modeling (QM/MM) studies have proposed several mechanisms for substrate activation and water oxidation in the OEC of PSII.[5,21,22,35,36] Although there have been detailed proposals for the mechanism of solar water oxidation in PSII, there is little experimental data available on the structure of the bound water molecules in the OEC of PSII. Further, there is also a lack of structural data on the bound water molecules in the higher S-state photochemical intermediates of the catalytic Mn_4Ca–oxo cluster. This is especially difficult as the higher S-states are transient and have limited stability. While X-ray absorption spectroscopy is highly sensitive to the location of the metal ions, it is not suited to probe the location of the water molecules in the OEC. Other techniques, such as FTIR and conventional EPR spectroscopy, have yielded limited information. While these studies have enhanced our knowledge of the structure and function of the OEC, there are several crucial questions that are yet to be answered and there is an urgent need for detailed investigations using advanced spectroscopic techniques.

Electron paramagnetic resonance (EPR) spectroscopy has been successfully used to probe the geometric and electronic structure of the Mn_4Ca–oxo cluster in the S-state intermediates of the OEC. It is a powerful tool as the Mn_4Ca–oxo cluster is paramagnetic in the S_0–S_4 photochemical intermediates. Among the S-state intermediates, the S_2 state is of particular interest as it represents the next transition in the catalytic S-state cycle after the dark stable S_1 state. The important structural questions that warrant immediate attention with respect to the S_2 state are: (i) the precise location and binding of the substrate water molecules, (ii) the protonation state of the substrate water molecules, (iii) the oxidation state of the manganese ions that ligate the substrate water molecules and (iv) the molecular structure of the Mn_4Ca–oxo cluster, namely, the geometry of the cluster, the magnetic coupling scheme of the metal ions and the electron spin density distribution among the four manganese ions in the Mn_4Ca–oxo

cluster. It is especially significant that EPR spectroscopy can provide an important means to probe these vital questions.

It has previously been possible to obtain certain geometric and electronic parameters of the Mn_4Ca–oxo cluster by the analysis of conventional field-swept EPR spectra in frozen solutions. However, weak 'through space' magnetic hyperfine couplings between the Mn_4Ca–oxo cluster and surrounding nuclei (such as protons of the bound substrate water molecules) are obscured in the frozen solutions due to inhomogeneous line broadening. Advanced EPR techniques such as electron nuclear double resonance (ENDOR)[37–39] and electron spin echo envelope modulation (ESEEM) spectroscopy are designed to overcome this problem.[40,41] However, it is a major challenge to interpret the experimental data that are obtained by ESEEM and ENDOR spectroscopy as these methods simultaneously detect the presence of multiple nuclei in the vicinity of the Mn_4Ca–oxo cluster which results in severe superposition of spectral features from the different nuclei.

In comparison with one-dimensional (1D) EPR spectroscopy methods, the use of two-dimensional (2D) EPR methods, such as hyperfine sub-level correlation (HYSCORE) spectroscopy, simplifies the detection and analysis of multiple electron–nuclear interactions. This is because in 2D HYSCORE spectroscopy the overlapping nuclear frequencies are separated in a second dimension and there is a correlation of nuclear frequencies that arise from different electron spin manifolds.[42] Although HYSCORE spectroscopy suffers from intrinsic limitations, such as the presence of blind spots and more importantly a much longer data acquisition time that is required for the experiment, enhanced resolution with respect to simultaneous detection of multiple nuclei provides significant advantages for the study of paramagnetic centers that have complex structures such as OEC.

Among the magnetic nuclei surrounding the paramagnetic core of the OEC, protons are of particular interest as these are naturally abundant. Importantly, protons serve as natural probes to observe structural changes of the substrate water molecules in the OEC. Further, protons have a large magnetic moment in comparison with other magnetic nuclei that renders them as highly sensitive probes of the OEC. The direct determination of the strength and nature of the electron–nuclear couplings arising from the protons can provide valuable information on the location, geometry and activation of the substrate water molecules. In addition, the detection of protons through the paramagnetic Mn_4Ca–oxo cluster of the OEC exclusively selects for the water molecules that are directly coordinated at the catalytic Mn_4Ca–oxo in the OEC.

The pioneering research by Kawamori and coworkers using continuous-wave ENDOR (cw ENDOR) spectroscopy allowed, for the first time, the detection of multiple proton hyperfine interactions of the S_2 state.[43] The observation of the proton hyperfine interactions provided direct evidence that protons are located in the vicinity of the Mn_4Ca–oxo cluster. Subsequent studies using cw ENDOR spectroscopy confirmed the close proximity of protons but provided a different interpretation of the observed hyperfine splittings.[44,45] A rigorous analysis of the proton hyperfine interactions in the S_2 state of the OEC has been conducted by Britt and coworkers.[32,46] The authors applied pulsed ENDOR spectroscopy in combination with ESEEM spectroscopy to provide evidence that at least one water molecule is directly coordinated to a manganese ion in the S_2 state and a second water molecule is proximal to the Mn_4Ca–oxo cluster. In the absence of an X-ray crystal structure of PSII, these early studies provided significant insight on the structure of the OEC of PSII.

In the present study, we use 2D ^{1}H HYSCORE spectroscopy in conjunction with the photochemical capture of the S_2 state of the OEC to detect the substrate water molecules that are coordinated in the OEC of PSII. We study the electron–nuclear hyperfine couplings in the S_2 state of the OEC to identify the presence of proton (nuclear spin $I = 1/2$) couplings to the S_2 state (electron spin $S = 1/2$) of the Mn_4Ca–oxo cluster. In this study, the presence of the second dimension in frequency space increases the spectral resolution thus allowing for the separation of the spectral features belonging to different nuclei in the OEC. We compare the experimental data obtained in this study with previous data on model systems that mimic the S_2 state of the OEC. Based on the recently reported 1.9 Å resolution X-ray structure of the OEC in the S_1 state, we make important conclusions about the location and structure of the substrate water molecules in the S_2 state of the OEC of PSII.

Materials and methods

Preparation of photosystem II complexes

Preparation of photosystem II complexes from the PsbB variant of *Synechocystis* PCC 6803. The hexa-histidine-tagged (HT) PsbB variant of *Synechocystis* PCC 6803 (a mesophilic cyanobacterium) was prepared by minor modification of previously published procedures.[47] The PsbB variant of *Synechocystis* PCC 6803 was grown on agar plates containing BG-11 medium (1.76 M sodium nitrate ($NaNO_3$), 30.3 mM magnesium sulfate ($MgSO_4$), 24.5 mM calcium chloride ($CaCl_2$), 3.14 mM citric acid and a mixture containing boric acid (H_3BO_3), manganese chloride ($MnCl_2$), zinc sulfate ($ZnSO_4$), molybdic acid (H_2MoO_4), cupric sulfate ($CuSO_4$) and cobalt nitrate ($Co(NO_3)_2$)).[48] The single colonies of the PsbB variant of *Synechocystis* PCC 6803 were harvested from the BG-11 agar plates, sub-cultured to 100 ml growths and propagated to 18 l liquid cultures under constant illumination at ~30 °C using liquid BG-11 medium with 5 mM glucose and 5 mM 2-[[1,3-dihydroxy-2-(hydroxymethyl)propan-2-yl]amino]ethanesulfonic acid/potassium hydroxide ((TES)-KOH) at pH 8.2.[48] The cells were harvested by continuous-flow filtration (Millipore, Billerica, MA) and resuspended in buffer containing 50 mM 2-(*N*-morpholino)ethanesulfonic acid/sodium hydroxide (MES-NaOH) at pH 6.0, 5 mM $CaCl_2$, 5 mM magnesium chloride ($MgCl_2$) and 25% w/v glycerol. The cells were broken using a bead-beater (BioSpec, Bartlesville, OK) and the thylakoids were separated by ultracentrifugation. The thylakoids were used to prepare a dodecyl-β-D-maltoside (β-DM)-solubilized extract of proteins in buffer containing 50 mM MES-NaOH, pH 6.0, 20 mM $CaCl_2$, 5 mM $MgCl_2$, 25% (w/v) glycerol and 0.03% (w/v) β-DM. The protein extract was subjected to purification on a Ni^{2+}-metal affinity chromatography column (Qiagen, Valencia, CA) to isolate highly pure HT–PSII complexes.[47] The isolation and purification procedures were conducted in the dark at 4 °C. The resulting HT–PSII complexes were monitored by SDS-polyacrylamide gel electrophoresis and

the densitometry scans showed very minor PSI contamination (<3%). The O_2-evolution rates were monitored by a Clark electrode and were typically 4800 μmol of O_2 per mg of Chl h^{-1}.[49]

Preparation of photosystem II complexes from *Thermosynechococcus vulcanus*. Highly pure PSII dimer core complexes were obtained from a thermophilic cyanobacterium, *Thermosynechococcus vulcanus* (*T. vulcanus*) according to a previously established protocol,[50,51] with slight modifications. The cells were grown at 50–53 °C while bubbling of air containing 5% (v/v) CO_2. The crude PSII obtained after treatment of thylakoids with lauryldimethylamine *N*-oxide was solubilized with 1.0% β-DM, and then loaded onto a Q Sepharose high performance column (GE Healthcare) pre-equilibrated with a solution containing 30 mM MES (pH 6.0), 3 mM $CaCl_2$, and 0.03% β-DM. The PSII monomers and dimers were separated with a linear gradient of 170–300 mM NaCl in the same solution, and the fraction containing PSII dimer was collected, diluted two-fold with the same solution without β-DM, and then precipitated by centrifugation following the addition of polyethylene glycol (PEG) 1450 (Sigma-Aldrich) to a final concentration of 13%. The precipitated dimers were suspended in 30 mM MES, 3 mM $CaCl_2$, 20 mM NaCl at pH 6.0 and stored at 77 K in the dark.

To perform exchange with deuterated buffer, the PSII dimers were washed twice after incubating for six hours in buffer prepared in deuterated water, D_2O, with 30 mM MES (pH = 6.0), 3 mM $CaCl_2$, 20 mM NaCl and 30% deuterated glycerol.

Preparation of photosystem II membranes from spinach. PSII membranes were isolated from market spinach using modifications of previously published procedures.[52] The intact thylakoid membranes that were prepared from market spinach were resuspended in a buffer containing 20 mM *N*-(2-hydroxyethyl) piperazine-*N*′-2-ethanesulfonic acid (HEPES), 15 mM sodium chloride (NaCl), 4 mM $MgCl_2$, 1 mM sodium 2,2′,2″,2‴-(ethane-1,2-diyldinitrilo)tetraacetate (EDTA) and 1 mg ml^{-1} bovine serum albumin (BSA) at pH 7.5. The sub-chloroplast membranes were isolated from the thylakoids by incubation with triton X-100 for 20 minutes at 4 °C in a buffer containing 15 mM NaCl, 20 mM MES, 5 mM $MgCl_2$, 1 mM EDTA, 1 mg ml^{-1} BSA and one pinch of catalase at pH 6.0. The sub-chloroplast membranes were washed repeatedly with the above buffer and were resuspended in buffer with triton X-100. The isolation and purification procedures were conducted in the dark at 4 °C. The resulting PSII membranes were monitored by SDS-polyacrylamide gel electrophoresis. The O_2-evolution rates were monitored by a Clark electrode and were typically 600–650 μmol of O_2 per mg of Chl h^{-1}.[49]

To perform exchange with deuterated buffer, the PSII membranes were washed twice after incubating for three hours and twenty-four hours in buffer prepared in deuterated water, D_2O, with 20 mM MES (pH = 6.0), 15 mM NaCl, 5 mM $MgCl_2$ and 30% deuterated ethylene glycol.

Trapping of the S_2 state photochemical intermediate

The cyanobacterial PSII complexes used for the EPR and 2D HYSCORE measurements of the S_2 and S_1 states of the OEC were resuspended in buffer containing 50 mM MES-NaOH, 20 mM $CaCl_2$, 5 mM $MgCl_2$, 0.03% (w/v) β-DM and 30% glycerol (w/v) at pH 6.0. The PSII samples were preincubated with 200 μM potassium ferricyanide prior to illumination. The S_2 state was cryo-trapped by illumination for 2 minutes at 200 K followed by rapid freezing (5–10 s) at 77 K in the dark.[49] The S_1 state was accumulated by dark-adapting the PSII sample at 0 °C for 30 minutes.

The PSII membranes from spinach were resuspended in buffer containing 15 mM NaCl, 20 mM MES, 5 mM $MgCl_2$, 1 mM EDTA, 1 mg ml^{-1} BSA and one pinch of catalase at pH 6.0. The PSII membranes were preincubated with 200 μM potassium ferricyanide prior to illumination. The S_2 state was cryo-trapped by illumination for 2 minutes at 200 K followed by rapid freezing (5–10 s) at 77 K in the dark. Once again, the S_1 state was accumulated by dark-adapting the PSII membranes at 0 °C for 30 minutes.

Pulsed EPR spectroscopy

The EPR spectra were recorded on a custom-built continuous-wave (cw)/pulsed X-band Bruker Elexsys 580 spectrometer. The pulsed EPR measurements were conducted with a dielectric flex-line probe ER 4118-MD5 (Bruker BioSpin Corporation, Billerica, MA) and a dynamic continuous-flow cryostat CF935 (Oxford Instruments, Oxfordshire, UK). The operating microwave frequency was set to 9.71 GHz to best match the broad band of the strongly over-coupled pulsed resonator. All of the pulsed EPR spectra were acquired at 5 K.

For the electron spin-echo-detected magnetic field-sweep EPR spectra, the primary electron spin echo was generated using the pulse sequence ($\pi/2$–τ–π–echo). The echo was integrated over a 40 ns time window that was centered at the maximum of the echo signal. The length of the $\pi/2$- and π-pulse was 12 ns and 24 ns, respectively. The inter-pulse separation, τ, was 144 ns and the delay in the pulse sequence is defined as the difference in the starting point of the pulses.

For the 2D HYSCORE spectra, the echo amplitude was measured using the pulse sequence ($\pi/2$–τ–$\pi/2$–t_1–π–t_2–$\pi/2$–echo) with an 8 ns and 16 ns length for the $\pi/2$- and π-pulse, respectively, and an 8 ns detector gate (that is centered at the maximum of the echo signal). The delays in the pulse sequence are defined as the difference in the starting point of the pulses. The echo intensity was measured as a function of t_1 and t_2, where t_1 and t_2 were incremented in steps of 16 ns from an initial value of 40 ns and 32 ns, respectively. 256 steps were used for each dimension. The 8 ns time difference between the initial value of t_1 and t_2 was set to account for the difference in length between the $\pi/2$- and π-pulses. This provided symmetric spectra in both dimensions. The unwanted echoes and anti-echoes were eliminated by applying a 16-step phase cycling procedure. A third order polynomial baseline was subtracted from the resulting time-domain spectra. The corrected spectra were zero-filled to obtain [2048 × 2048] matrix and Fourier transformed using a Fast Fourier Transformation (FFT) algorithm. The frequency domain spectra were plotted as the amplitudes (absolute value) of the 2D frequency components.

The ^{1}H HYSCORE spectra were recorded at magnetic field of 337.5 mT (effective g = 1.95) with an inter-pulse delay, τ, of 140 ns (this is the delay between the first and the second pulse). The choice of the inter-pulse delay was mandatory, since useful

spectral information can only be obtained if the contribution due to matrix nuclei is suppressed by matching the blind-spot frequency to the proton Zeeman frequency ($\nu_Z = 14.37$ MHz). To match the blind-spot frequency and the proton Zeeman frequency, the inter-pulse delay, τ, must satisfy the condition $\tau = N/\nu_Z$ (where $N = 1, 2, 3, \ldots$), thus τ has to be $N \times 70$ ns. Since a τ value of 70 ns is too short to avoid the ring down of the resonator, the shortest τ that yields practical results is 140 ns. If the condition, $\tau = N/\nu_Z$, is not matched there is an intense matrix proton signal that dominates the 2D ^{1}H HYSCORE spectrum that masks important structural information. An example is shown in Fig. S1‡ using a τ value of 176 ns (please see ESI‡ section).

Results

Spin-echo-detected magnetic field-sweep EPR spectra of the S_2 state of photosystem II

The illumination of PSII at 200 K results in the advancement of the oxygen-evolving complex from the S_1 to the S_2 state.[53–56] Shown in Fig. 1A–C are the S_2-minus-S_1 spin-echo-detected magnetic field-sweep EPR difference spectra of PSII that were isolated and purified from (a) a thermophilic cyanobacterium, *Thermosynechococcus vulcanus* (*T. vulcanus*), (b) a mesophilic cyanobacterium, the PsbB variant of *Synechocystis* PCC 6803 and (c) higher plants, namely, spinach. We observe a multiline EPR spectral pattern centered at $g \approx 2$ that confirms the presence of the S_2 state of the OEC in all three of the PSII samples.[53–56] The multiline EPR spectrum arises from the magnetic coupling of the paramagnetic Mn_4Ca–oxo cluster in the S_2 state (electron spin $S = ½$) and the nuclear spin ($I = 5/2$) of the four ^{55}Mn ions.[53–56] In addition to the light induced S_2 state we observe signals from the dark-stable tyrosyl radical ($Y_D^{\cdot}$) and the primary semiquinone Q_A^- that is magnetically coupled to the high-spin non-heme Fe(II) center of PSII.[57] We do not observe a contribution from the oxidized heme center of Cyt b_{559} in the S_2-minus-S_1 difference EPR spectra of PSII as Cyt b_{559} was completely pre-oxidized in the S_1 state. The spectral contributions from the $Y_D^{\cdot}$ and Q_A^- centers are easily avoided in the acquisition of the 2D HYSCORE spectra by selecting magnetic field position(s) that correspond to an effective g-value of 1.95, where the spin-echo-detected magnetic-field-sweep EPR signal from the S_2 state of the OEC has maximum intensity.

2D ^{1}H HYSCORE spectra of the S_2 state of photosystem II

Shown in Fig. 2 is a complete 2D HYSCORE spectrum of the S_2 state of the OEC of PSII from *T. vulcanus*. The spectrum was obtained at a magnetic field position corresponding to $g = 1.95$ which is marked by an arrow in Fig. 1. We observe spectral features in both the (−, +) and (+, +) quadrants of the 2D HYSCORE spectrum due to magnetic couplings of the paramagnetic Mn_4Ca–oxo cluster in the S_2 state (electron spin $S = ½$) with the nuclear spin of the surrounding ^{14}N ($I = 1$) and ^{1}H ($I = ½$) atoms. We have previously reported analysis of the spectral features arising from the electron–nuclear hyperfine couplings of the Mn_4Ca–oxo cluster in the S_2 state with the ^{14}N atoms in the OEC of PSII from the PsbB variant of *Synechocystis* PCC 6803.[57] In the present study, we discuss the hyperfine couplings of the Mn_4Ca–oxo cluster in the S_2 state with protons in the OEC of PSII from *T. vulcanus*, the PsbB variant of *Synechocystis* PCC 6803 and spinach, respectively.

The 2D ^{1}H HYSCORE spectrum of the S_2 state of the OEC of PSII from *T. vulcanus* is shown in Fig. 3. We observe multiple cross-peaks (or ridges) in the (+, +) quadrant of the 2D ^{1}H HYSCORE spectrum that are symmetrically positioned at the

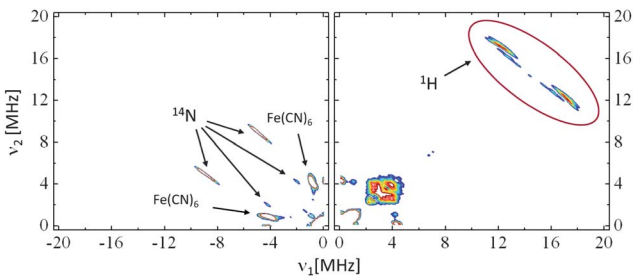

Fig. 2 The (−, +) and (+, +) quadrants of the 2D HYSCORE spectrum of the S_2 state of the OEC of PSII from *T. vulcanus* in protonated buffer. The spectrum was acquired at a magnetic field position corresponding to a g value of 1.95 with a τ delay of 140 ns.

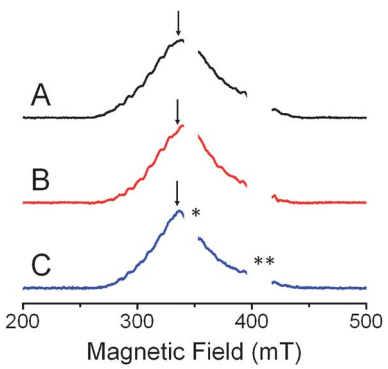

Fig. 1 The pulsed spin-echo-detected magnetic-field-sweep EPR spectra of the S_2 state of the OEC of PSII from (A) *T. vulcanus*, (B) the PsbB variant of *Synechocystis* PCC 6803 and (C) spinach. * The region of the spectrum containing the EPR signal from the $Y_D^{\cdot}$ radical. ** The region of the spectrum containing unavoidable resonator artifacts.

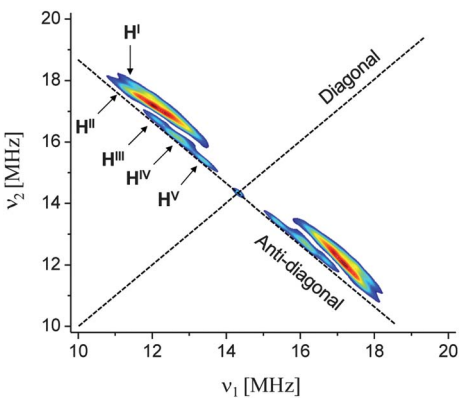

Fig. 3 The 2D ^{1}H HYSCORE spectrum of the S_2 state of the OEC of PSII from *T. vulcanus* in protonated buffer. The spectrum was acquired at a magnetic field position corresponding to a g value of 1.95 with a τ delay of 140 ns.

proton Zeeman frequency of 14.37 MHz. Hence, the ridges are easily recognized as arising from the electron–nuclear hyperfine interaction of the Mn_4Ca–oxo cluster in the S_2 state with neighboring protons in the OEC. The 2D ^{1}H HYSCORE spectrum displays five resolved ridges from hyperfine interactions with distinct groups of protons, H^I–H^V (marked in Fig. 3). Two of the ridges, H^I and H^{II}, are strongly shifted from the anti-diagonal (the anti-diagonal is defined as $\nu_1 + \nu_2 = 2\nu_Z$, where ν_Z = 14.37 MHz). The shift from the anti-diagonal is due to 'through space' dipolar interactions indicating the presence of significant anisotropic hyperfine interactions with the H^I and H^{II} group of protons. The other ridges arising from the H^{III}–H^V groups of protons display a much smaller shift from the anti-diagonal indicating a smaller anisotropic dipolar contribution to the hyperfine interaction. However, the three groups of protons, H^{III}–H^V, exhibit significant differences in the shift of their respective ridges from the main diagonal (the main diagonal is defined as $\nu_1 - \nu_2 = 0$). The shift from the main diagonal is caused by the isotropic Fermi contact interaction that is proportional to the electron spin density of the corresponding nucleus. The ridge arising from the hyperfine coupling with the H^{III} group of protons has a much larger shift from the diagonal that indicates a significant isotropic contribution to the hyperfine interaction. All of the groups of protons, H^I–H^V, are unambiguously assigned to originate from hyperfine interactions of the S_2 state of the OEC as these interactions are absent in the dark-adapted S_1 state of the OEC. Shown in Fig. S2 (please see ESI‡) are the skyline projection plots of the 2D ^{1}H HYSCORE spectra of the S_1 and S_2 state of the OEC (please refer to Fig. S3 in the ESI‡ section for the complete 2D HYSCORE spectrum). As can be seen in Fig. S2A‡, we only observe a small spectral contribution that arises from non-specific hyperfine interactions with the matrix protons in the dark-adapted S_1 state of the OEC.

The 2D ^{1}H HYSCORE spectra of the S_2 state of the OEC of PSII from the PsbB variant of *Synechocystis* PCC 6803 and spinach are shown in Fig. S4 and S5, respectively (please see ESI‡ section). Although the spectral resolution of the 2D ^{1}H HYSCORE spectra of the S_2 state in Fig. S4 and S5‡ is slightly lower than the resolution of the corresponding 2D ^{1}H HYSCORE spectrum that is obtained from the S_2 state of the OEC of PSII from *T. vulcanus*, we observe that the proton hyperfine couplings are very similar in the S_2 state of the OEC of PSII from the three species.

The position of the proton ridges in the 2D frequency space is determined by the anisotropic and isotropic hyperfine components of the electron–nuclear hyperfine tensor. From the slope and the intercept in the frequency-squared coordinates, we determine the anisotropic (T) and isotropic (a_{iso}) hyperfine components for each of the five groups of protons that contribute to the 2D ^{1}H HYSCORE spectrum in Fig. 3. The details of the quantitative analysis are presented in the ESI‡ section. The hyperfine couplings that are obtained from the numerical analysis are listed in Table 1.

Table 1 The hyperfine interaction parameters of the ^{1}H nuclei obtained by spectral simulations of the 2D ^{1}H HYSCORE spectrum of the S_2 state of PSII shown in Fig. 3

Ridge	T, MHz	a_{iso}, MHz
H^I	±4.4 (±0.3)	±1.8 (±0.4)
H^{II}	±4.1 (±0.3)	±0.1 (±0.4)
H^{III}	±1.9 (±0.2)	±2.6 (±0.2)
H^{IV}	±2.3 (±0.2)	±0.2 (±0.2)
H^V	±1.4 (±0.4)	±0.4 (±0.6)

Discussion

The electron–nuclear hyperfine interaction is highly sensitive to the geometric and electronic structure of the paramagnetic center. The anisotropic component of the hyperfine interaction is determined by the through space dipolar interaction and it is inversely proportional to the cube of the inter-spin distance ($1/r^3$, where r is the distance) between the nucleus and unpaired electron. In the case of the paramagnetic Mn_4Ca–oxo cluster of the OEC, the anisotropic component of the hyperfine interaction, T, is determined by the superposition of the magnetic fields that are induced by the four manganese ions. Therefore, the anisotropic component depends on both the geometry and the electron spin density distribution within the cluster. In contrast, the isotropic component of the hyperfine interaction is induced through the Fermi contact interaction and serves as a measure of the extent of involvement of the nucleus in a chemical bond with the cluster.

In order to assign the distinct groups of protons, H^I–H^V, that contribute to the experimental 2D ^{1}H HYSCORE spectrum, we examine the hyperfine parameters that are obtained in this study in conjunction with the recent high-resolution X-ray crystal structure of the OEC of PSII in the S_1 state[24] and pulsed EPR spectroscopy studies of mixed-valence manganese models that mimic the S_2 state of the Mn_4Ca–oxo cluster.[58–61] Although the recent high-resolution X-ray crystal structure of PSII was obtained in the S_1 state of the OEC,[24] only subtle structural changes of the Mn_4Ca–oxo cluster have been suggested during the S_1 to S_2 transition.[23,62]

In order to assign the H^I–H^V groups of protons, we have to consider all of the structural units containing protons that are within 5 Å of the Mn_4Ca–oxo cluster in the OEC. This yields the following possibilities, (i) the amino acid ligands that are directly coordinated to the Mn_4Ca–oxo cluster, namely, D1-Glu189, D1-Asp170, D1-Glu333, D1-Asp342, D1-Ala344, CP43-Glu354 and D1-His332; (ii) the amino acid side chains that are not directly coordinated to the Mn_4Ca–oxo cluster, namely, D1-His337, D1-Tyr161, CP43-Arg357, D1-Gln165, D1-Val185, D1-Asp61 and D1-Ser169; (iii) the two water molecules that are coordinated to the Mn4 ion in the Mn_4Ca–oxo cluster (PDB ID: 3ARC),[24] namely, W999A and W1000A (corresponding to W2, W1, respectively, in ref. 24); (iv) the two water molecules that are coordinated to the Ca^{2+} ion in the Mn_4Ca–oxo cluster (PDB ID: 3ARC),[24] namely, W540A and W541A (W4, W3 in ref. 24) and (v) nine water molecules that form a hydrogen bond network in the vicinity of the Mn_4Ca–oxo cluster (PDB ID: 3ARC),[24] namely, W428A, W442A, W446A, W538C, W539A, W542A, W543A, W548C and W923A.[63]

The protons on the carboxylic acid side chains of the amino acid residues, D1-Glu189, D1-Asp170, D1-Glu333, D1-Asp342, CP43-Glu354 and D1-Asp61, are at least four bonds removed from the manganese ions of the Mn_4Ca–oxo cluster which precludes detection by 2D ^{1}H HYSCORE spectroscopy. This is

strongly supported by recent 2D ^{1}H HYSCORE spectroscopy studies of the dimanganese di-μ-oxo terpyridine model complex in the presence of acetate ions.[58] In this case, when an acetate ion is directly coordinated to the Mn(III) ion, the distance to the most proximal methyl protons on the acetate ion is too large to be detected by 2D ^{1}H HYSCORE spectroscopy. Thus, in order to assign the H^I–H^V group of protons, we only consider protons of the four water molecules that are coordinated at the manganese and calcium ions of the cluster, the nine water molecules in the hydrogen bond network and the D1-His332, D1-His337 and CP43-Arg357 residues, respectively, that are in the vicinity of the Mn_4Ca–oxo cluster as shown in Fig. 4.

Assignment of the H^I group of protons

We assign the H^I group of protons to a water molecule that is directly coordinated at a manganese ion in the Mn_4Ca–oxo cluster. The large anisotropic component of the hyperfine interaction, T, of ±4.4 MHz (Table 1) indicates that the proton(s) are in very close proximity to the Mn_4Ca–oxo cluster in the S_2 state of the OEC. More importantly, the magnitude of the isotropic component of the hyperfine interaction, a_{iso}, of ±1.8 MHz indicates that the proton(s) are involved in a chemical bond with the Mn_4Ca–oxo cluster. The value of a_{iso} that is obtained for the H^I group of protons is in excellent agreement with the values of a_{iso} that are obtained for the protons of a water ligand that is coordinated either to a Mn(III) or Mn(IV) ion of mixed-valence Mn(III)–Mn(IV) model complexes.[58,61] The value of a_{iso} rapidly decreases upon bond number separation from the manganese ion and it was found to be smaller than ~1 MHz for the protons of the terpyridine and bipyridine ligand of the model complexes.[58,59] Thus, based on the value of a_{iso} we exclude the possibility that the H^I group of protons is due to water molecules that are not directly coordinated to a manganese ion in the Mn_4Ca–oxo cluster or the ring protons of the D1-His332 residue.

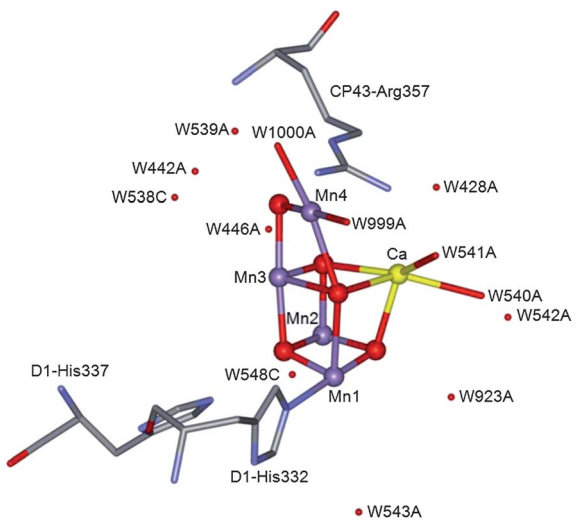

Fig. 4 The structure of the Mn_4Ca–oxo cluster as observed in the X-ray crystal structure of PSII.[24] Shown are the protons of the four water molecules that are coordinated at the manganese and calcium ions of the cluster, the nine water molecules in the hydrogen bond network and the D1-His332, D1-His337 and CP43-Arg357 residues, respectively, that are in the vicinity of the Mn_4Ca–oxo cluster.

The value of T depends on the distance of the corresponding proton to each of the manganese ions and the respective spin projection factors p_i (where $i = 1, 2, 3, 4$) of the manganese ions in the Mn_4Ca–oxo cluster. Using a simple point dipole approximation with a spin projection factor of $p_4 = 1$ and neglecting contributions from the other manganese ions in the cluster yields a distance of 2.6 Å between the protons on the water molecule and the Mn4 ion in the S_2 state of the OEC of PSII. This is in excellent agreement with the X-ray crystal structure of the OEC in the S_1 state for two water molecules, W999A and W1000A, directly coordinated at the Mn4 ion (Fig. 4).[24]

Assignment of the H^{II} group of protons

We assign the H^{II} group of protons to either the two protons of the D1-His332 ligand that is proximal to the Mn1 ion or protons from either of the two water molecules that are coordinated at the Ca^{2+} ion, W540A and W541A, in the Mn_4Ca–oxo cluster in the S_2 state of the OEC (Fig. 4). The presence of a negligible isotropic hyperfine interaction, a_{iso}, in Table 1 indicates that the H^{II} group of protons is not due to water molecules that are directly coordinated to a manganese ion in the Mn_4Ca–oxo cluster. However, the value of T indicates that the H^{II} group of protons is in close proximity to at least one of the manganese ions in the cluster.

There are three possibilities for the assignment of the H^{II} group of protons: (i) the two water molecules that are coordinated to the Ca^{2+} ion in the cluster, (ii) the two ring protons from the D1-His332 residue that is ligated to the cluster or (iii) the amino proton of the D1-His337 residue that is H-bonded to the oxygen atom that bridges the Mn1, Mn2 and Mn3 ions (Fig. 4). Since we observe a nearly axial hyperfine tensor for H^{II}, we exclude the amino proton of the D1-His337 residue that is H-bonded to the cluster. For a proton that is H-bonded to a μ-oxo bridge of the Mn_4Ca–oxo cluster, we expect the presence of a highly rhombic hyperfine interaction.

One of the water molecules that is bound to the Ca^{2+} ion, namely W541A, and the two ring protons of D1-His332 are located at a reasonable distance from Mn_4Ca–oxo cluster to explain the value of T of ±4.1 MHz. However, we tend to favor the assignment of the H^{II} group of protons to the two ring protons of the D1-His332 residue. This is because the hyperfine parameters of H^{II} are nearly identical to the hyperfine parameters that were obtained for the two protons of the terpyridine ligand coordinated at the Mn(III) ion of the dimanganese di-μ-oxo terpyridine model complex.[58] The two protons of the D1-His332 residue are nearly symmetric with respect to the Mn1 ion at a distance of ~3.15 Å (Fig. 4). Further, the relative geometry and bond structure between the Mn1 ion and the two proximal protons of D1-His332 are nearly identical to the protons of the dimanganese di-μ-oxo terpyridine model complex. Although the X-ray crystal structure yields only the location of the Mn1 ion, the oxidation state of the manganese ion has been identified as Mn(III) by pulsed EPR spectroscopy.[64,65]

Assignment of the H^{III} group of protons

We assign the H^{III} group of protons to a water molecule that is directly coordinated to a manganese ion, Mn4, in the

Mn_4Ca–oxo cluster. The value of a_{iso} in Table 1 clearly indicates that H^{III} is due to a water ligand of one of the manganese ions in the cluster. Interestingly, the value of T for the H^{III} group of protons is smaller than the value of T that was observed for the H^{I} group. Using a simple point-dipole approximation with a spin projection factor of 1 yields a distance of ~3.5 Å which might appear large for a directly bound water ligand. However, we have to take into account that the magnitude of T is determined by superposition of the magnetic fields that are induced by all four manganese ions of the cluster. The hyperfine parameters that are obtained for H^{III} closely match the hyperfine interaction of the water ligand coordinated at the Mn(IV) ion of the dimanganese di-μ-oxo terpyridine model complex.[58] The smaller value of T that was measured for the protons of the water ligand of the model complex is due to the influence of the Mn(III) ion that is connected with the Mn(IV) ion through a di-μ-oxo bridge. The Mn(III) ion that is antiferromagnetically coupled to the Mn(IV) ion has a spin projection factor that is opposite in sign to the spin projection factor of the Mn(IV) ion. This reduces the total magnetic field that is experienced by the water protons. Although the distance from the water ligand to the Mn(III) ion is much longer, the spin projection factor of the Mn(III) ion is twice as large in comparison with that of the Mn(IV) ions. This results in a significant contribution to the measured value of T. Based on the hyperfine parameters of H^{III}, we conclude that there is a structural similarity between the water ligand attributed to H^{III} that is bound at the Mn4 ion (oxidation state Mn(IV)) and a water ligand that is coordinated at the Mn(IV) ion of the dimanganese di-μ-oxo terpyridine model complex.[58]

Interestingly, the value of T for the H^{I} and H^{III} group of protons is significantly different. The difference is too large to assign H^{I} and H^{III} to the same water molecule. In the X-ray crystal structure of PSII, there are two water ligands W999A and W1000A that are directly coordinated to the Mn4 ion in the Mn_4Ca–oxo cluster (Fig. 4). In order to explain the smaller value of T for the H^{III} group of protons, the presence of at least one other Mn ion in close proximity to Mn4 with an opposite sign of the spin projection factor is required. According to the X-ray crystal structure, only the Mn3 ion is proximal enough to explain the smaller value of T for the H^{III} group of protons. However, the geometry of both of the water molecules is similar in the X-ray crystal structure and this does not explain the large difference in the values of T for H^{I} and H^{III}. Thus, our data indicate that the structure of the S_2 state is different from the S_1 state. The experimental 2D ^{1}H HYSCORE data obtained in the present study indicate that there is more asymmetry with respect to the water molecules in the S_2 state of the OEC. Such an asymmetry could be introduced by a rearrangement of the OEC upon the S_1 to S_2 state transition.

It is important to note that at present, there is a lack of experimental evidence to draw firm conclusions on the protonation state of the water ligands that are coordinated at the manganese ions in the Mn_4Ca–oxo cluster. Thus, it is possible that H^{I} and/or H^{III} could be due to a hydroxyl group. However, we disfavor this possibility since the observed values of a_{iso} are in excellent agreement with the protonated water ligands that were detected in the 2D ^{1}H HYSCORE spectra of the dimanganese di-μ-oxo terpyridine model complex. Also, for a hydroxyl group we expect a much stronger covalency of the Mn–O bond that would likely result in a significantly larger value of a_{iso}.

Assignment of the H^{IV} group of protons

There are multiple possibilities for the assignment of the H^{IV} group of protons. The negligible value of a_{iso} for the H^{IV} protons suggests that these protons could belong to a water molecule that is not directly coordinated to the manganese ions and is located at a distance of ~4 Å. The other possibility is that these protons belong to the amino acids that are in the proximity of the Mn_4Ca–oxo cluster, namely, the D1-His337 or CP43-Arg357 residues in the OEC as shown in Fig. 4.

Assignment of the H^{V} group of protons

We assign the H^{V} group of protons to multiple hyperfine interactions with remote matrix protons. The very small values of the hyperfine components clearly indicate that these protons are not located in close proximity to the Mn_4Ca–oxo cluster. Further, the intensity of the 2D ^{1}H HYSCORE cross-peaks is significantly diminished for weakly interacting protons. Thus, even though several protons contribute to the H^{V} ridge in the 2D ^{1}H HYSCORE spectrum, the observed intensity is relatively small. The H^{V} group of protons does not carry significant structural information.

Comparison of the OEC of photosystem II from cyanobacteria and higher plants

A comparison between the structure of PSII from cyanobacteria and spinach is very important since numerous complementary experimental studies have been conducted on these organisms. The hyperfine interactions between the Mn_4Ca–oxo paramagnetic core and the surrounding protons are highly sensitive probes of changes in the geometric and electronic structure of the OEC of PSII. The position of the ridges of the 2D ^{1}H HYSCORE spectrum in 2D frequency space is strictly determined by electron–nuclear hyperfine interaction parameters. For the S_2 state of the OEC, we detect five distinct groups of protons surrounding the Mn_4Ca–oxo cluster. The H^{I}–H^{III} group of protons is assigned to the first coordination sphere of the Mn_4Ca–oxo cluster: H^{I} and H^{III} are protons of water molecules directly bound at the Mn ions and H^{II} is either two proximal protons of D1-His332 residue or the water ligands coordinated at the Ca^{2+} ion.

The presence of structural differences in the electronic structure of the OEC would result in observable changes of the 2D ^{1}H HYSCORE spectrum of the S_2 state. The redistribution of electron spin density or distortion of the geometry of the Mn_4Ca–oxo cluster would affect the anisotropic hyperfine components through a change of spin projection factors, distances and angles to individual manganese ions. A careful comparison of the 2D ^{1}H HYSCORE spectra of the S_2 state of the OEC of PSII from *T. vulcanus*, the PsbB variant of *Synechocystis* PCC 6803 and spinach shown in Fig. 3, S4 and S5‡, respectively, does not reveal observable differences in the position of the ridges arising from hyperfine interactions with the H^{I}–H^{V} group of protons. The hyperfine parameters of the H^{I}–H^{V} group of protons are identical to within ~10%. This allows us to

firmly conclude that the structural differences in the OEC of PSII from the three species are indeed negligible.

In the recent pulsed EPR study, Messinger and coworkers compared ^{55}Mn ENDOR spectra of PSII from cyanobacteria and spinach.[66] Similar to the present study, the authors did not detect significant differences in the electronic structure of the manganese ions of the OEC of PSII from *T. elongatus* and spinach.

Comparison with previous EPR spectroscopy studies

The hyperfine interactions between the paramagnetic Mn_4Ca–oxo cluster and the surrounding protons in the S_2 state of the OEC have been the subject of previous studies. Kawamori and coworkers have reported the presence of six pairs of hyperfine interactions in the OEC,[43] of which two of the largest splittings were suggested to arise from exchangeable protons. In contrast, subsequent studies reported four proton hyperfine interactions in the OEC.[44,45] More recent studies have reproduced the results obtained by Kawamori and coworkers.[31]

All of these studies were performed by the application of cw ENDOR spectroscopy. Despite the similarities of the hyperfine parameters that have been reported in these studies, the interpretation of the experimental spectra is significantly different. A hyperfine interaction with a single proton might result in the appearance of three cw ENDOR splittings corresponding to the three principal components of the hyperfine tensor. However, in the presence of multiple protons, severe superposition of the peaks precludes clear assignments. Therefore, cw ENDOR spectra are difficult to interpret and it is not possible to determine unambiguous assignments of proton hyperfine interactions. For nearly axial interactions, the parallel component of the hyperfine tensor would be very hard to detect by ENDOR due to its low statistical weight. If we assume that only perpendicular components of the hyperfine tensor are detected in the cw ENDOR experiments, then according to our data given in the Table 1 one should observe five hyperfine splittings: 0.7 MHz, ~1 MHz, 2.1 MHz, 2.6 MHz and 4.0 MHz. This is in good agreement with previous cw ENDOR measurements.

A rigorous investigation using a combination of pulsed ^{1}H ENDOR and ^{2}H ESEEM spectroscopy has also been reported in the literature.[32] In this study, the authors investigate the ENDOR spectrum of the S_2 state of PSII in protonated buffer and the 1D ^{2}H ESEEM spectrum of the S_2 state of PSII that was exchanged in deuterated buffer. The experimental data are interpreted in terms of four groups of protons/deuterons that are interacting with the paramagnetic Mn_4Ca–oxo cluster in the S_2 state of the OEC. Although the use of a combination of pulsed EPR spectroscopy methods enhances the quality of the analysis, both ^{1}H ENDOR and 1D ^{2}H ESEEM spectroscopy do not resolve the individual contributions of multiple protons/deuterons. Thus, these methods do not provide a direct measure of the number of different hyperfine tensors that contribute to the observed experimental spectra. Moreover, in the case of ^{2}H ESEEM spectroscopy the variables in the numerical simulations include the individual quadrupole tensors and the three Euler angles that characterize the relative orientation of each tensor. Thus, interpretations of the experimental data are indeed very complex. Even though the authors used ^{1}H ENDOR spectroscopy as an additional constraint for evaluating the unknown parameters, the interpretation contains a certain degree of uncertainty. Despite uncertainties in previous studies, the results reported in the pulsed ENDOR and 1D ESEEM spectroscopy study are in agreement with the results of this study for four groups of protons. The first and second groups of protons agree with the H^{I} and H^{II} groups listed in Table 1. The third group agrees with the H^{IV} and the fourth group with the H^{V} group of protons.

Since 2D ^{1}H HYSCORE spectroscopy resolves different nuclei due to the presence of a second dimension it is well suited for the study of multinuclear paramagnetic centers. A recent 2D ^{1}H HYSCORE spectroscopy study of the S_2 state of OEC in spinach PSII has suggested hyperfine interactions from two groups of protons.[67] The values of the isotropic and anisotropic components that were reported for the hyperfine interaction with the first group are 0.6 MHz and 2.9 MHz and with the second group 0.3 MHz and 6.7 MHz, respectively. These results contradict the values of the hyperfine parameters that are listed in Table 1.[67]

Conclusions

In this work, we use 2D ^{1}H HYSCORE spectroscopy to study the weak magnetic interactions of the paramagnetic Mn_4Ca–oxo cluster and the surrounding protons in the S_2 state of the OEC of PSII from three different species namely, *T. vulcanus*, the PsbB variant of *Synechocystis* PCC 6803 and spinach. We observe five well-resolved groups of protons, H^{I}–H^{V}, that are interacting with the Mn_4Ca–oxo cluster in the S_2 state of the OEC. For each group of protons, we determine isotropic and anisotropic components of the hyperfine tensor, a_{iso} and T, respectively, that are presented in Table 1. Based on the values of the hyperfine parameters, we assign two groups of protons, H^{I} and H^{III}, to water ligands directly coordinated at the manganese ion(s) of the Mn_4Ca–oxo cluster in the S_2 state of the OEC. The hyperfine parameters suggest that H^{II} is located in close proximity to at least one of the manganese ions. Therefore, we assign H^{II} to either the two proximal protons of D1-His332 residue or the water ligands coordinated at the Ca^{2+} ion. Further spectroscopic investigations are required to discriminate between the two possibilities. Multiple assignments are possible for the H^{IV} group of protons and H^{V} is assigned to ambient water molecules and/or remote protons from neighboring amino acid residues. We observe negligible differences in the 2D ^{1}H HYSCORE spectra of the S_2 state of the OEC of PSII from *T. vulcanus*, the PsbB variant of *Synechocystis* PCC 6803 and spinach. This suggests a high homology of the OEC across the three species. The proton hyperfine parameters presented in this study provide an important means to refine theoretical models of the S_2 state of the OEC of PSII.

Acknowledgements

This research is supported by the Photosynthetic Systems Program, Office of Basic Energy Sciences, United States Department of Energy (DE-FG02-07ER15903). The authors thank Professor Gary Brudvig and Professor Victor Batista for helpful discussions on the OEC of PSII.

References

1 R. E. Blankenship, *Molecular Mechanisms of Photosynthesis*, Wiley-Blackwell, 2002.
2 J. P. McEvoy and G. W. Brudvig, *Chem. Rev.*, 2006, **106**, 4455–4483.
3 D. G. Nicholls and S. J. Ferguson, *Bioenergetics 3*, Academic Press, New York, 2002.
4 R. E. Blankenship, *Photosynth. Res.*, 1992, **33**, 91–111.
5 P. E. M. Siegbahn, *Acc. Chem. Res.*, 2009, **42**, 1871–1880.
6 J. Kern and G. Renger, *Photosynth. Res.*, 2007, **94**, 183–202.
7 R. J. Debus, *Biochim. Biophys. Acta, Bioenerg.*, 1992, **1102**, 269–352.
8 V. K. Yachandra, K. Sauer and M. P. Klein, *Chem. Rev.*, 1996, **96**, 2927–2950.
9 B. Kok, B. Forbush and M. McGloin, *Photochem. Photobiol.*, 1970, **11**, 457–475.
10 A. Zouni, H. T. Witt, J. Kern, P. Fromme, N. Krauss, W. Saenger and P. Orth, *Nature*, 2001, **409**, 739–743.
11 N. Kamiya and J. R. Shen, *Proc. Natl. Acad. Sci. U. S. A.*, 2003, **100**, 98–103.
12 K. N. Ferreira, T. M. Iverson, K. Maghlaoui, J. Barber and S. Iwata, *Science*, 2004, **303**, 1831–1838.
13 B. Loll, J. Kern, W. Saenger, A. Zouni and J. Biesiadka, *Nature*, 2005, **438**, 1040–1044.
14 J. M. Peloquin and R. D. Britt, *Biochim. Biophys. Acta, Bioenerg.*, 2001, **1503**, 96–111.
15 J. Messinger, J. H. A. Nugent and M. C. W. Evans, *Biochemistry*, 1997, **36**, 11055–11060.
16 K. A. Ahrling, S. Peterson and S. Styring, *Biochemistry*, 1998, **37**, 8115–8120.
17 L. V. Kulik, B. Epel, W. Lubitz and J. Messinger, *J. Am. Chem. Soc.*, 2005, **127**, 2392–2393.
18 H. A. Chu, W. Hillier, N. A. Law and G. T. Babcock, *Biochim. Biophys. Acta, Bioenerg.*, 2001, **1503**, 69–82.
19 R. J. Debus, *Coord. Chem. Rev.*, 2008, **252**, 244–258.
20 J. Yano, Y. Pushkar, P. Glatzel, A. Lewis, K. Sauer, J. Messinger, U. Bergmann and V. Yachandra, *J. Am. Chem. Soc.*, 2005, **127**, 14974–14975.
21 E. M. Sproviero, J. A. Gascon, J. P. McEvoy, G. W. Brudvig and V. S. Batista, *Curr. Opin. Struct. Biol.*, 2007, **17**, 173–180.
22 E. M. Sproviero, J. A. Gascon, J. P. McEvoy, G. W. Brudvig and V. S. Batista, *Coord. Chem. Rev.*, 2008, **252**, 395–415.
23 J. Yano, J. Kern, K. Sauer, M. J. Latimer, Y. Pushkar, J. Biesiadka, B. Loll, W. Saenger, J. Messinger, A. Zouni and V. K. Yachandra, *Science*, 2006, **314**, 821–825.
24 Y. Umena, K. Kawakami, J. R. Shen and N. Kamiya, *Nature*, 2011, **473**, 55–60.
25 A. Guskov, J. Kern, A. Gabdulkhakov, M. Broser, A. Zouni and W. Saenger, *Nat. Struct. Mol. Biol.*, 2009, **16**, 334–342.
26 S. Luber, I. Rivalta, Y. Umena, K. Kawakami, J.-R. Shen, N. Kamiya, G. W. Brudvig and V. S. Batista, *Biochemistry*, 2011, **50**, 6308–6311.
27 Y. L. Pushkar, J. Yano, K. Sauer, A. Boussac and V. K. Yachandra, *Proc. Natl. Acad. Sci. U. S. A.*, 2008, **105**, 1879–1884.
28 H. A. Chu, W. Hillier and R. J. Debus, *Biochemistry*, 2004, **43**, 3152–3166.
29 T. Noguchi, T. Ono and Y. Inoue, *Biochemistry*, 1992, **31**, 5953–5956.
30 T. Noguchi and M. Sugiura, *Biochemistry*, 2001, **40**, 1497–1502.
31 H. Yamada, H. Mino and S. Itoh, *Biochim. Biophys. Acta, Bioenerg.*, 2007, **1767**, 197–203.
32 R. D. Britt, K. A. Campbell, J. M. Peloquin, M. L. Gilchrist, C. P. Aznar, M. M. Dicus, J. Robblee and J. Messinger, *Biochim. Biophys. Acta, Bioenerg.*, 2004, **1655**, 158–171.
33 J. H. Su and J. Messinger, *Appl. Magn. Reson.*, 2010, **37**, 123–136.
34 J. Yano, J. Kern, Y. Pushkar, K. Sauer, P. Glatzel, U. Bergmann, J. Messinger, A. Zouni and V. K. Yachandra, *Philos. Trans. R. Soc. London, Ser. B*, 2008, **363**, 1139–1147.
35 E. M. Sproviero, J. A. Gascon, J. P. McEvoy, G. W. Brudvig and V. S. Batista, *J. Am. Chem. Soc.*, 2008, **130**, 3428–3442.
36 P. E. M. Siegbahn, *Curr. Opin. Struct. Biol.*, 2002, **6**, 227–235.
37 G. Feher, *Phys. Rev.*, 1956, **103**, 834–835.
38 E. R. Davies, *Phys. Lett. A*, 1974, **47**, 1–2.
39 W. B. Mims, *Proc. R. Soc. London, Ser. A*, 1965, **283**, 452–457.
40 A. Schweiger and G. Jeschke, *Principles of Pulse Electron Paramagnetic Resonance*, Oxford University Press, 2001.
41 S. A. Dikanov and Y. D. Tsvetkov, *Electron Spin Echo Modulation (ESEEM) Spectroscopy*, CRC Press, Inc., 1992.
42 P. Hofer, A. Grupp, H. Nebenfuhr and M. Mehring, *Chem. Phys. Lett.*, 1986, **132**, 279–282.
43 A. Kawamori, T. Inui, T. Ono and Y. Inoue, *FEBS Lett.*, 1989, **254**, 219–224.
44 X. S. Tang, M. Sivaraja and G. C. Dismukes, *J. Am. Chem. Soc.*, 1993, **115**, 2382–2389.
45 R. Fiege, W. Zweygart, R. Bittl, N. Adir, G. Renger and W. Lubitz, *Photosynth. Res.*, 1996, **48**, 227–237.
46 C. P. Aznar and R. D. Britt, *Philos. Trans. R. Soc. London, Ser. B*, 2002, **357**, 1359–1365.
47 K. V. Lakshmi, M. J. Reifler, D. A. Chisholm, J. Y. Wang, B. A. Diner and G. W. Brudvig, *Photosynth. Res.*, 2002, **72**, 175–189.
48 R. Rippka, J. Deruelles, J. B. Waterbury, M. Herdman and R. Y. Stanier, *J. Gen. Microbiol.*, 1979, **111**, 1–61.
49 W. F. Beck, J. C. Depaula and G. W. Brudvig, *Biochemistry*, 1985, **24**, 3035–3043.
50 J. R. Shen and Y. Inoue, *Biochemistry*, 1993, **32**, 1825–1832.
51 J. R. Shen and N. Kamiya, *Biochemistry*, 2000, **39**, 14739–14744.
52 D. A. Berthold, G. T. Babcock and C. F. Yocum, *FEBS Lett.*, 1981, **134**, 231–234.
53 J. C. Depaula, W. F. Beck and G. W. Brudvig, *J. Am. Chem. Soc.*, 1986, **108**, 4002–4009.
54 M. Zheng and G. C. Dismukes, *Inorg. Chem.*, 1996, **35**, 3307–3319.
55 G. W. Brudvig, *Adv. Chem.*, 1995, **246**, 249–263.
56 G. W. Brudvig, *ACS Symp. Ser.*, 1988, **372**, 221–237.
57 S. Milikisiyants, R. Chatterjee, A. Weyers, A. Meenaghan, C. Coates and K. V. Lakshmi, *J. Phys. Chem. B*, 2010, **114**, 10905–10911.
58 S. Milikisiyants, R. Chatterjee and K. V. Lakshmi, *J. Phys. Chem. B*, 2011, **115**, 12220–12229.
59 D. W. Randall, M. K. Chan, W. H. Armstrong and R. D. Britt, *Mol. Phys.*, 1998, **95**, 1283–1294.
60 K. O. Schafer, R. Bittl, W. Zweygart, F. Lendzian, G. Haselhorst, T. Weyhermuller, K. Wieghardt and W. Lubitz, *J. Am. Chem. Soc.*, 1998, **120**, 13104–13120.
61 D. W. Randall, A. Gelasco, M. T. Caudle, V. L. Pecoraro and R. D. Britt, *J. Am. Chem. Soc.*, 1997, **119**, 4481–4491.
62 K. Sauer, J. Yano and V. K. Yachandra, *Coord. Chem. Rev.*, 2008, **252**, 318–335.
63 K. Kawakami, Y. Umena, N. Kamiya and J.-R. Shen, *J. Photochem. Photobiol., B*, 2011, **104**, 9–18.
64 C. Teutloff, S. Pudollek, S. Kessen, M. Broser, A. Zouni and R. Bittl, *Phys. Chem. Chem. Phys.*, 2009, **11**, 6715–6726.
65 T. A. Stich, J. W. Whittaker and R. D. Britt, *J. Phys. Chem. B*, 2010, **114**, 14178–14188.
66 J.-H. Su, N. Cox, W. Ames, D. A. Pantazis, L. Rapatskiy, T. Lohmiller, L. V. Kulik, P. Dorlet, A. W. Rutherford, F. Neese, A. Boussac, W. Lubitz and J. Messinger, *Biochim. Biophys. Acta, Bioenerg.*, 2011, **1807**, 829–840.
67 J. I. Martinez, I. Yruela, R. Picorel and P. J. Alonso, *J. Phys. Chem. B*, 2010, **114**, 15345–15353.

